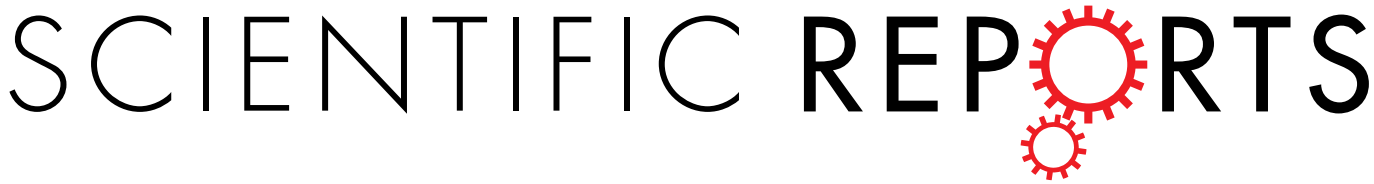

OPEN

Pure spin-Hall magnetoresistance in $Rh/Y_3Fe_5O_{12}$ hybrid

T. Shang[1], Q. F. Zhan[1], L. Ma[2], H. L. Yang[1], Z. H. Zuo[1], Y. L. Xie[1], H. H. Li[1], L. P. Liu[1], B. M. Wang[1], Y. H. Wu[3], S. Zhang[4] & Run-Wei Li[1]

Received: 06 October 2015
Accepted: 05 November 2015
Published: 07 December 2015

We report an investigation of anisotropic magnetoresistance (AMR) and anomalous Hall resistance (AHR) of Rh and Pt thin films sputtered on epitaxial $Y_3Fe_5O_{12}$ (YIG) ferromagnetic insulator films. For the Pt/YIG hybrid, large spin-Hall magne toresistance (SMR) along with a sizable conventional anisotropic magnetoresistance (CAMR) and a nontrivial temperature dependence of AHR were observed in the temperature range of 5–300 K. In contrast, a reduced SMR with negligible CAMR and AHR was found in Rh/YIG hybrid. Since CAMR and AHR are characteristics for all ferromagnetic metals, our results suggest that the Pt is likely magnetized by YIG due to the magnetic proximity effect (MPE) while Rh remains free of MPE. Thus the Rh/YIG hybrid could be an ideal model system to explore physics and devices associated with pure spin current.

The studies of magnetic insulator-based spintronics have recently generated great interest due to their segregated characteristic of spin current from charge current[1]. The interplay between spin and charge transports in nonmagnetic metal/ferromagnetic insulator (NM/FMI) hybrids gives rise to various interesting phenomena, such as spin injection[2,3], spin pumping[4–6], and spin Seebeck[7,8]. The previous investigations on NM/FMI hybrids, e.g., $Pt/Y_3Fe_5O_{12}$ (Pt/YIG), also demonstrated a new-type of magnetoresistance[9–13] in which the resistivity of films, ρ, has an unconventional angular dependence, namely,

$$\rho = \rho_0 - \Delta\rho\,[\hat{\mathbf{m}} \cdot (\hat{\mathbf{z}} \times \hat{\mathbf{j}})]^2 \quad (1)$$

where $\hat{\mathbf{m}}$ and $\hat{\mathbf{j}}$ are unit vectors in the directions of the magnetization and the electric current, respectively, and $\hat{\mathbf{z}}$ represents the normal vector perpendicular to the plane of the film; ρ_0 is the zero-field resistivity. The above angular-dependent resistivity has been named as the spin-Hall magnetoresistance (SMR) in order to differentiate from the conventional anisotropic magnetoresistance (CAMR) in which $\rho = \rho_0 + \Delta\rho\,(\hat{\mathbf{m}} \cdot \hat{\mathbf{j}})^2$. A theoretical model outlined below has been proposed to explain the SMR. An electric current $(\mathbf{j}_e)$ induces a spin current due to the spin-Hall effect and in turn, the induced spin current, via inverse spin-Hall effect, generates an electric current whose direction is opposite to the original current[14–21]. Thus , the combined spin-Hall and inverse spin-Hall effects lead to an additional resistance in bulk materials with spin-orbit coupling (SOC). However, in an ultra-thin film, the spin current could be either reflected back at the interface or absorbed at the interface through spin transfer torque. In the former case, the total spin current in the metal layer is reduced and thus the additional resistance is minimized. The spin current reflection is strongest when the magnetization direction $\hat{\mathbf{m}}$ of the ferromagnetic insulator is parallel to the spin polarization $\hat{\mathbf{z}} \times \hat{\mathbf{j}}$ of the spin current, leading to the resistive minimum as described in Eq. (1)[14,15].

[1]Key Laboratory of Magnetic Materials and Devices & Zhejiang Province Key Laboratory of Magnetic Materials and Application Technology, Ningbo Institute of Material Technology and Engineering, Chinese Academy of Sciences, Ningbo, Zhejiang 315201, P. R. China. [2]Department of Physics, Tongji University, Shanghai, 200092, P. R. China. [3]Department of Electrical and Computer Engineering, National University of Singapore, 4 Engineering Drive 3 117583, Singapore. [4]Department of Physics, University of Arizona, Tucson, Arizona 85721, USA. Correspondence and requests for materials should be addressed to Q.F.Z. (email: zhanqf@nimte.ac.cn) or S.Z. (email: zhangshu@email.arizona.edu) or R.-W.L. (email: runweili@nimte.ac.cn)

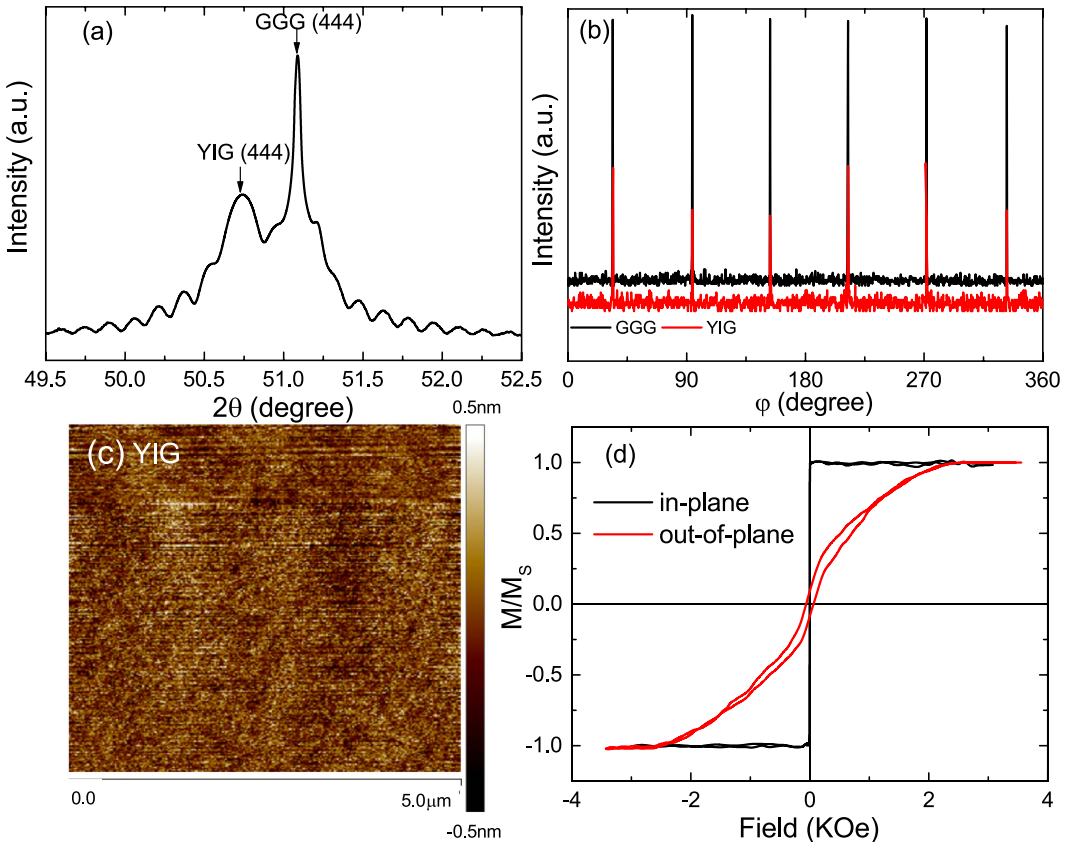

Figure 1. (**a**) A representative $2\theta-\omega$ XRD patterns for YIG/GGG film near the (444) peaks of GGG substrate and YIG film. (**b**) The φ-scan of YIG/GGG film. (**c**) AFM surface topography of a representative YIG film. (**d**) The field dependence of normalized magnetization for YIG/GGG film measured at room temperature. For the in-plane (out-of-plane) magnetization, the magnetic field is applied parallel (perpendicular) to the film surface.

However, the magnetic proximity effect (MPE), in which a non-magnetic metal develops a sizable magnetic moment in the close vicinity of a ferromagnetic layer, may complicate the interpretation of the SMR. Pt is near the Stoner ferromagnetic instability and could become magnetic when in contact with ferromagnetic materials, as experimentally shown by x-ray magnetic circular dichroism (XMCD), anomalous Hall resistance (AHR), spin pumping, and first principle calculations of the Pt/YIG hybrid[22–26]. In order to separate the MPE from the pure SMR, many attempts have been made. By inserting a layer of Au or Cu between NM and FMI, the MPE can be effectively screened, but the SMR amplitude is largely suppressed as well[9,10]. Furthermore, the insertion of an extra layer would introduce an additional interface whose quality is not easily accessible. An alternative approach to pursue the pure SMR is to find proper NM metals in direct contact with YIG, but without the MPE. The Au has a SOC strength comparable to Pt or Pd and it is free of the MPE, but it has an extremely weak inverse spin-Hall voltage and SMR[26,27]. According to the theoretical calculation[28], the 4*d* metal Rh also possesses a large SOC strength and spin-Hall conductivity, and a small magnetic susceptibility, implying an insignificant MPE in the Rh metal when in contact with ferromagnetic materials. Thus Rh might be an excellent material for the pure SMR study.

In this article, the anisotropic magnetoresistance (AMR) and AHR of Rh/YIG and Pt/YIG hybrids were investigated in the temperature range of 5–300 K. Indeed, we show that the differences in magneto-transport properties between these two hybrids are attributed to the strong (Pt) and weak (Rh) MPE, and thus, Rh/YIG provides an ideal model system for pure spin-current investigations.

Results

Figure 1(a) plots a representative room-temperature $2\theta-\omega$ XRD scan of epitaxial YIG/GGG thin film near the (444) reflections of gadolinium gallium garnet (GGG) substrate and YIG film. Clear Laue oscillations indicate the flatness and uniformity of the epitaxial YIG film. The epitaxial nature of YIG film was characterized by φ-scan measurements with a fixed 2θ value at the (642) reflections, as shown in Fig. 1(b). In this study, the thicknesses of YIG and Rh or Pt films, determined by fitting the x-ray

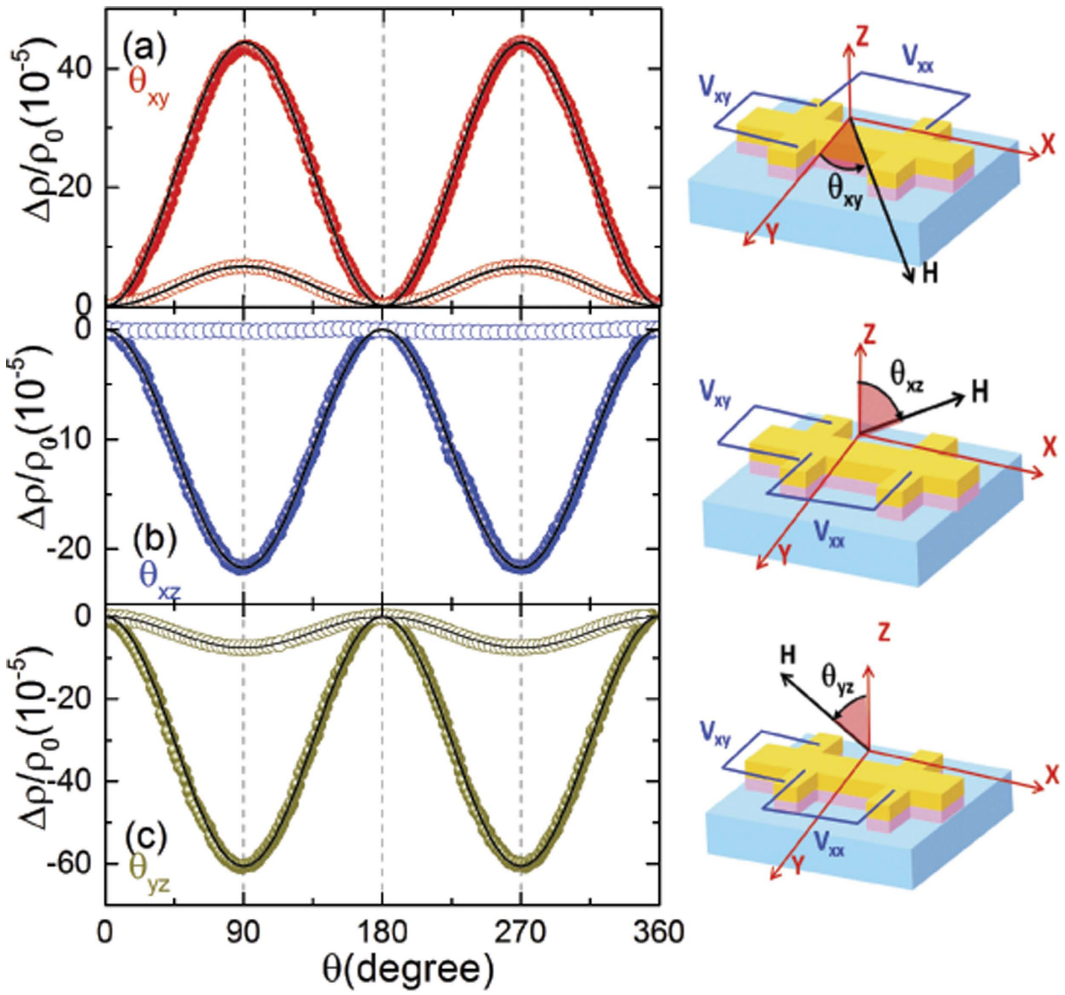

Figure 2. Anisotropic magnetoresistance for the Rh/YIG (open symbols) and Pt/YIG (closed symbols) hybrids with the magnetic field scanning within the *xy* (**a**), *xz* (**b**), and *yz* (**c**) planes. The AMR is measured at room temperature in a field of $\mu_0 H = 20$ kOe. The solid lines through the data are fits to $\cos^2\theta$ with a 90 degree phase shift. The right panels show the schematic plots of longitudinal resistance and transverse Hall resistance measurements and notations of different field scans in the patterned Hall bar hybrids. The θ_{xy}, θ_{xz}, and θ_{yz} denote the angles of the applied magnetic field relative to the *y*-, *z*-, and *z*-axes, respectively.

reflectivity (XRR) spectra, are approximately 50 nm and 3 nm, respectively. The AFM surface topography of a representative YIG film in Fig. 1(c) reveals a surface roughness of 0.15 nm, indicating atomically flat of the epitaxial YIG film. As shown in Fig. 1(d), the in-plane and out-of-plane coercivities of the YIG film are <1 Oe and 60 Oe, respectively. The paramagnetic background of the GGG substrate has been subtracted and the magnetization is normalized to the saturation magnetization M_s. The out-of-plane magnetization saturates at a field above 2.2 kOe, which is consistent with previous results[12,22]. The above properties indicate the excellent quality of our epitaxial YIG film.

Figure 2(a–c) plot the room-temperature AMR for the Rh/YIG (open symbols) and Pt/YIG (closed symbols) hybrids. As shown in the right panels, the Rh/YIG and Pt/YIG hybrids are patterned into Hall-bar geometry and the electric current is applied along the *x*-axis. The AMR is measured in a magnetic field of 20 kOe, which is sufficiently strong to rotate the YIG magnetization in any direction. Here the total AMR is defined as $\Delta\rho/\rho_0 = [\rho(M\|I) - \rho(M\perp I)]/\rho_0$. We note that when the magnetic field scans within the *xy* plane [Fig. 2(a)], both the CAMR and SMR contribute to the total AMR, and it is difficult to separate them from each other; for the *xz* plane [Fig. 2(b)], the magnetization of YIG is always perpendicular to the spin polarization of the spin current and the SMR is absent, and the resistance changes are attributed to the MPE-induced CAMR. For the *yz* plane [Fig. 2(c)], the electric current is always perpendicular to the magnetization, the CAMR is zero, and only the SMR survives. According to Eq. (1), the amplitudes of CAMR or SMR ($\Delta\rho/\rho_0$) oscillate as a function of $\cos^2\theta$, as shown by the solid black lines in Fig. 2. Both the Rh/YIG and Pt/YIG hybrids display clear SMR at room temperature, with

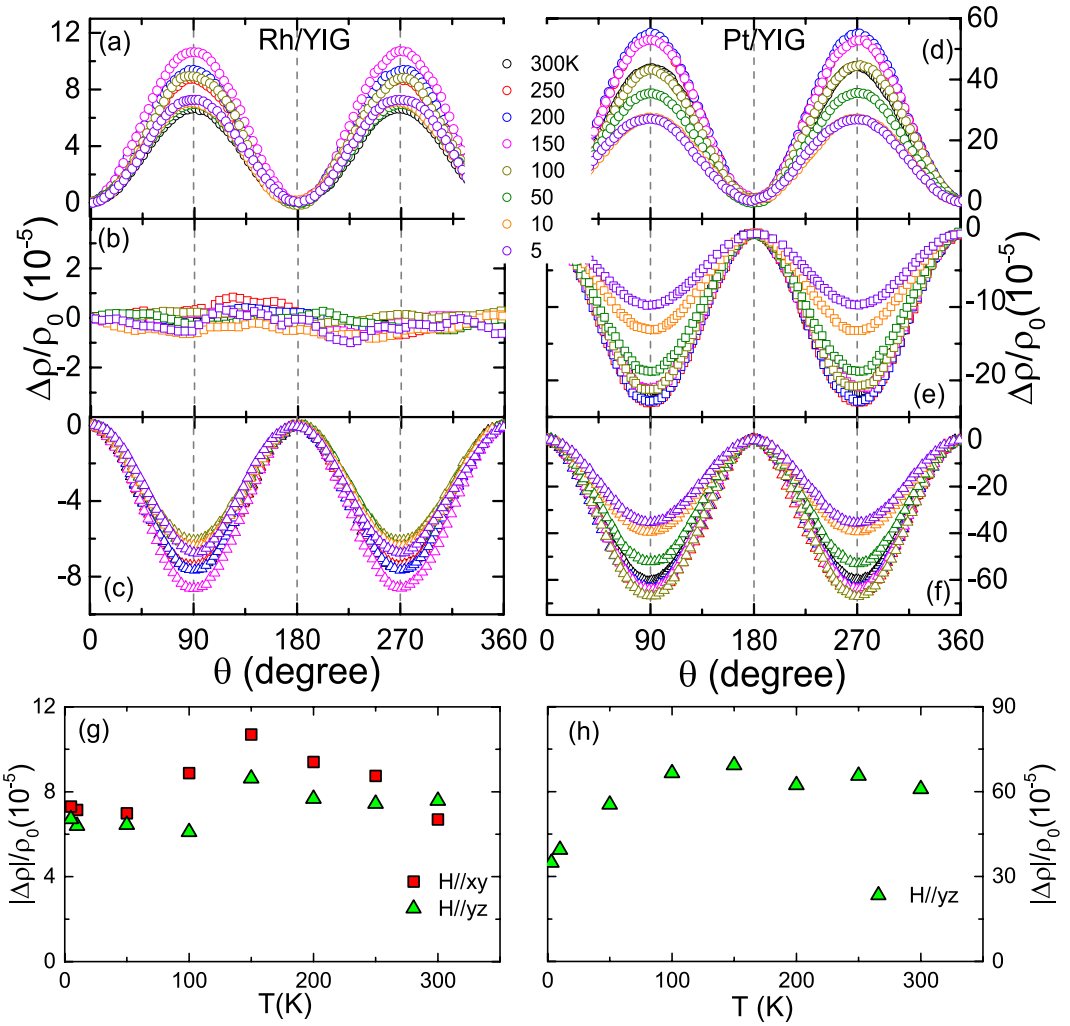

Figure 3. Anisotropic magnetoresistance for the Rh/YIG hybrid at various temperatures down to 5 K for the θ_{xy} (**a**), θ_{xz} (**b**), and θ_{yz} (**c**) scans. The results of Pt/YIG are shown in (**d**–**f**). The AMR is measured in a field of $\mu_0 H = 20$ kOe. (**g**,**h**) plot the temperature dependence of SMR amplitude for the Rh/YIG and Pt/YIG hybrids, respectively. The cubic and triangle symbols stand for the θ_{xy} and θ_{yz} scans, respectively.

the amplitudes reaching 7.6×10^{-5} and 6.1×10^{-4}, respectively [see Fig. 2(c)]. On the other hand, the CAMR also exists in the Pt/YIG, and its amplitude of 2.2×10^{-4} is comparable to the SMR. However, as shown in Fig. 2(b), for Rh/YIG hybrid, the θ_{xz} scan shows negligible AMR and the resistivity is almost independent of θ_{xz}, indicating the extremely weak MPE at the Rh/YIG interface in contrast to the significant effect at the Pt/YIG interface. The MPE at Pt/YIG interface was previously evidenced from the measurements of XMCD, AHR, and spin pumping[22,24,25].

Upon decreasing temperature, the SMR persists down to 5 K in both the Rh/YIG and Pt/YIG hybrids [see Fig. 3]. However, there is no sizable CAMR in the Rh/YIG hybrid down to the lowest temperature [see Fig. 3(b)], indicating the extremely weak MPE at the interface even at low temperature. While for the Pt/YIG hybrid, as shown in Fig. 3(e), the amplitude of CAMR is almost independent of temperature for $T > 100$ K, and then decreases by further lowering temperature, with the amplitude reaching 1.0×10^{-4} at 5 K. The above features are quite different from the Pd/YIG hybrid, where the amplitude of CAMR increases as the temperature decreases, showing a comparable value to the SMR at 3 K[12]. The reason for these different behaviors is unclear, and further investigations are needed. Since the CAMR is negligible in Rh/YIG, the SMR dominates the AMR when the magnetic field is varied within the *xy* plane. Figure 3(g,h) plot the temperature dependence of SMR amplitude for the Rh/YIG and Pt/YIG, respectively. The SMR amplitudes exhibit strong temperature dependence, reaching a maximum value of 1.1×10^{-4} (Rh/YIG) and 6.9×10^{-4} (Pt/YIG) around 150 K. Such nonmonotonic temperature dependence of SMR amplitude was previously reported in Pt/YIG hybrid, which can be described by a single spin-relaxation mechanism[29]. It is noted that the hybrids with different Rh thicknesses exhibit similar temperature dependent characteristics with different numerical values compared to the Rh(3 nm)/YIG

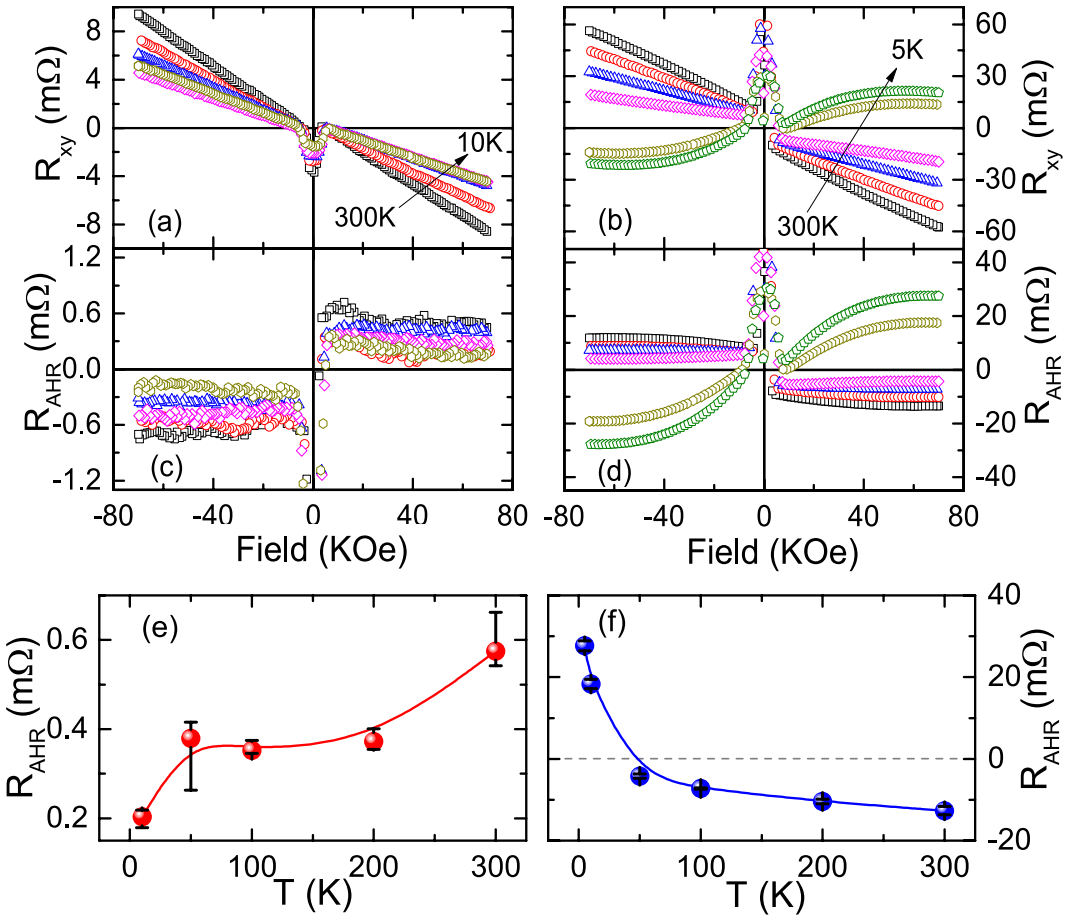

Figure 4. Transverse Hall resistance R_{xy} for the Rh/YIG (**a**) and Pt/YIG (**b**) hybrids as a function of magnetic field up to 70 kOe at different temperatures. The anomalous Hall resistance R_{AHR} for the Rh/YIG (**c**) and Pt/YIG (**d**) at different temperatures. The R_{AHR} can be derived by subtracting the linear background of OHR. Temperature dependence of R_{AHR} for the Rh/YIG (**e**) and Pt/YIG (**f**). All R_{AHR} are averaged by $[R_{AHR}(70\,kOe)- R_{AHR}(-70\,kOe)]/2$. The error bars are the results of subtracting OHR in different field ranges.

hybrid shown here. For example, the Rh(5 nm)/YIG hybrid reaches its maximum SMR amplitude of 0.8×10^{-4} around 100 K.

In order to characterize the MPE at the NM/FMI interface, we also carried out the measurements of transverse Hall resistance R_{xy} with a perpendicular magnetic field up to 70 kOe, as shown in Fig. 4(a,b). In both Rh and Pt thin films, the ordinary-Hall resistance (OHR), which is proportional to the external field, is subtracted from the measured R_{xy}, i.e., $R_{AHR} = R_{xy} - R_{OHR} \times \mu_0 H$, R_{AHR} is the anomalous Hall resistance. The resulting R_{AHR} as a function of magnetic field for the Rh/YIG and Pt/YIG hybrids are shown in Fig. 4(c,d), respectively. The AHR is proportional to the out-of-plane magnetization, and thus provides a notion for MPE at the NM/FMI interface. At room temperature, for the Rh/YIG hybrid, the $R_{AHR} = 0.57\,m\Omega$, which is 22 times smaller than the Pt/YIG hybrid, implying the extremely weak MPE at Rh/YIG interface, being consistent with the AMR results in Fig. 2(b). We note that the R_{AHR} of Rh/YIG hybrids with different Rh thicknesses was also measured. For example, the R_{AHR} reaches 1.65 mΩ and 0.26 mΩ in Rh(2 nm)/YIG and Rh(5 nm)/YIG at room temperature, respectively. The temperature dependence of R_{AHR} for the Rh/YIG and Pt/YIG hybrids are summarized in Fig. 4(e,f), respectively. As can be seen, the R_{AHR} exhibits significantly different behaviors: the R_{AHR} roughly decreases on lowering temperature in Rh/YIG. However, in Pt/YIG, the magnitude of R_{AHR} decrease with temperature for $T > 50$ K and then it suddenly increases upon further decreasing temperature. Moreover, the R_{AHR} of Pt/YIG changes sign below 50 K, while it is stays positive for Rh/YIG. Similar non-trivial AHR were also observed in Pt/LCO hybrids[30], but there is no existing quantitative theory to compare these results, further theoretical and experimental investigations are needed to clarify the dominating mechanisms.

Summary

In summary, we carried out measurements of angular dependence of magnetoresistance and transverse Hall resistance in Rh/YIG and Pt/YIG hybrids. Both hybrids exhibit SMR down to very low temperature. The observed AHR and CAMR indicate a significant MPE at the Pt/YIG interface, while it is negligible

at the Rh/YIG interface. Our findings suggest that the absence of the MPE makes the Rh/YIG bilayer system an ideal playground for pure spin-current related phenomena.

Methods

The Rh/YIG and Pt/YIG hybrids were prepared in a combined ultra-high vacuum (10^{-9} Torr) pulse laser deposition (PLD) and magnetron sputter system. The high quality epitaxial YIG thin films were grown on (111)-orientated single crystalline GGG substrate via PLD technique at 750 °C. The thin Rh and Pt films were deposited by magnetron sputtering at room temperature. All the thin films were patterned into Hall-bar geometry. The thickness and crystal structure were characterized by using Bruker D8 Discover high-resolution x-ray diffractometer (HRXRD). The thickness was estimated by using the software package LEPTOS (Bruker AXS). The surface topography and magnetic properties of the films were measured in Bruker Icon atomic force microscope (AFM) and Lakeshore vibrating sample magnetometer (VSM) at room temperature. The measurements of transverse Hall resistance and longitudinal resistance were carried out in a Quantum Design physical properties measurement system (PPMS-9 T) with a rotation option in a temperature range of 5–300 K.

References

1. Wu, M. Z. & Hoffmann, A. *Recent Advances in Magnetic Insulators - From Spintronics to Microwave Applications* (Academic Press, San Diego, Vol 64, 2013).
2. Ohno, Y. *et al.* Electrical spin injection in a ferromagnetic semiconductor heterostructure. *Nature* **402,** 790 (1999).
3. Jedema, F. J. *et al.* Electrical spin injection and accumulation at room temperature in an all-metal mesoscopic spin valve. *Nature* **410,** 345 (2001).
4. Heinrich, B. *et al.* Spin Pumping at the Magnetic Insulator (YIG)/Normal Metal (Au) Interfaces. *Phys. Rev. Lett.* **107,** 066604 (2011).
5. Rezende, S. M. *et al.* Enhanced spin pumping damping in yttrium iron garnet/Pt bilayers. *Appl. Phys. Lett.* **102,** 012402 (2013).
6. Kajiwara, Y. *et al.* Transmission of electrical signals by spin-wave interconversion in a magnetic insulator. *Nature* **464,** 262 (2010).
7. Uchida, K. *et al.* Observation of the spin Seebeck effect. *Nature* **455,** 778 (2008).
8. Uchida, K. *et al.* Spin Seebeck insulator. *Nat. Mater.* **9,** 894 (2010).
9. Miao, B. F. *et al.* Physical Origins of the New Magnetoresistance in Pt/YIG. *Phys. Rev. Lett.* **112,** 236601 (2014).
10. Althammer, M. *et al.* Quantitative study of the spin Hall magnetoresistance in ferromagnetic insulator/normal metal hybrids. *Phys. Rev. B* **87,** 224401 (2013).
11. Isasa, M. *et al.* Spin Hall magnetoresistance at Pt/$CoFe_2O_4$ interfaces and texture effects. *Appl. Phys. Lett.* **105,** 142402 (2014).
12. Lin, T. *et al.* Experimental Investigation of the Nature of the Magnetoresistance Effects in Pd-YIG Hybrid Structures. *Phys. Rev. Lett.* **113,** 037203 (2014).
13. Hahn, C. *et al.* Comparative measurements of inverse spin Hall effects and magnetoresistance in YIG/Pt and YIG/Ta. *Phys. Rev. B* **87,** 174417 (2013).
14. Nakayama, H. *et al.* Spin Hall Magnetoresistance Induced by a Nonequilibrium Proximity Effect. *Phys. Rev. Lett.* **110,** 206601 (2013).
15. Chen, Y. T. *et al.* Theory of spin Hall magnetoresistance. *Phys. Rev. B* **87,** 144411 (2013).
16. Hirsch, J. E. Spin Hall Effect. *Phys. Rev. Lett.* **83,** 1834 (1999).
17. Wunderlich, J. *et al.* Experimental Observation of the Spin-Hall Effect in a Two-Dimensional Spin-Orbit Coupled Semiconductor System. *Phys. Rev. Lett.* **94,** 047204 (2005).
18. Kato, Y. K. *et al.* Observation of the Spin Hall Effect in Semiconductors. *Science* **306,** 1910 (2004).
19. Saitoh, E. *et al.* Conversion of spin current into charge current at room temperature: Inverse spin-Hall effect. *Appl. Phys. Lett.* **88,** 182509 (2006).
20. Valenzuela, S. O. *et al.* Direct electronic measurement of the spin Hall effect. *Nature* **442,** 176 (2006).
21. Kimura, T. *et al.* Room-Temperature Reversible Spin Hall Effect. *Phys. Rev. Lett.* **98,** 156601 (2007).
22. Huang, S. Y. *et al.* Transport Magnetic Proximity Effects in Platinum. *Phys. Rev. Lett.* **109,** 107204 (2012).
23. Lin, T. *et al.* Induced magneto-transport properties at palladium/yttrium iron garnet interface. *Appl. Phys. Lett.* **103,** 132407 (2013).
24. Sun, Y. Y. *et al.* Damping in Yttrium Iron Garnet Nanoscale Films Capped by Platinum. *Phys. Rev. Lett.* **111,** 106601 (2013).
25. Lu, Y. M. *et al.* Pt Magnetic Polarization on $Y_3Fe_5O_{12}$ and Magnetotransport Characteristics. *Phys. Rev. Lett.* **110,** 147207 (2013).
26. Qu, D. *et al.* Intrinsic Spin Seebeck Effect in Au/YIG. *Phys. Rev. Lett.* **110,** 067206 (2013).
27. Wang, H. L. *et al.* Scaling of Spin Hall Angle in 3d, 4d, and 5d Metals from $Y_3Fe_5O_{12}$/Metal Spin Pumping. *Phys. Rev. Lett.* **112,** 197201 (2014).
28. Tanaka, T. *et al.* Intrinsic spin Hall effect and orbital Hall effect in 4d and 5d transition metals. *Phys. Rev. B* **77,** 165117 (2008).
29. Marmion, S. R. *et al.* Temperature dependence of spin Hall magnetoresistance in thin YIG/Pt films. *Phys. Rev. B* **89,** 220404(R) (2014).
30. Shang, T. *et al.* Extraordinary Hall resistance and unconventional magnetoresistance in Pt/$LaCoO_3$ hybrids. *Phys. Rev. B* **92,** 165114 (2015).

Acknowledgements

We acknowledge the fruitful discussions with S. M. Zhou. This work is financially supported by the National Natural Science Foundation of China (Grants No. 11274321, No. 11404349, No. 11174302, No. 51502314, No. 51522105) and the Key Research Program of the Chinese Academy of Sciences (Grant No. KJZD-EW-M05). S. Zhang was partially supported by the U. S. National Science Foundation (Grant No. ECCS-1404542).

Author Contributions

Q.F.Z., S.Z. and R.W.L. planned the experiments. T.S., L.M. and Y.L.X. synthesized the hybrids. Structure characterization, magnetic and transport measurements were performed by T.S., H.L.Y., Z.H.Z., H.H.L. and L.P.L. The data were analysed by T.S., H.L.Y., Y.H.W., B.M.W., Q.F.Z., S.Z. and R.W.L. T.S., Q.F.Z. and S.Z. wrote the paper. All authors participated in discussions and approved the submitted manuscript.

Additional Information

Competing financial interests: The authors declare no competing financial interests.

How to cite this article: Shang, T. *et al.* Pure spin-Hall magnetoresistance in $Rh/Y_3Fe_5O_{12}$ hybrid. *Sci. Rep.* **5**, 17734; doi: 10.1038/srep17734 (2015).